J Therm Anal Calorim
DOI 10.1007/s10973-017-6198-3

Thermal behaviour of antiproliferative active 3-(2-furanyl)-8-aryl-7,8-dihydroimidazo[2,1-*c*][1,2,4]triazin-4(6*H*)-ones

Agata Bartyzel[1] · Małgorzata Sztanke[2] · Krzysztof Sztanke[2,3]

Received: 21 December 2016 / Accepted: 15 February 2017

Abstract Thermal analysis is commonly used in the pharmaceutical field because it is an important tool in the solution of problems involving development, production and quality control of medicines. This paper presents the thermal behaviour of six anticancer active derivatives of 3-(2-furanyl)-8-aryl-7,8-dihydroimidazo[2,1-*c*][1,2,4]triazin-4(6*H*)-one. The samples were characterized by the TG–DSC and TG–FTIR analyses. The studied compounds are stable at room temperature which is important for medical application. The TG analysis under dynamic air atmosphere revealed that thermal degradation of the compounds starts above 300 °C and proceeds in two steps. The melting processes of compounds are observed before starting their decomposition or at the beginning of their combustion. Pyrolysis processes under nitrogen atmosphere take place in single or two steps. The major pyrolysis gaseous products identified are ammonia, carbon dioxide, isocyanic acid and its derivatives, hydrogen cyanide, aniline or its derivatives and carbon monoxide.

Keywords Anticancer agents · Fused 1,2,4-triazinones · Thermal studies · TG–DSC · TG–FTIR

✉ Agata Bartyzel
agata.bartyzel@poczta.umcs.lublin.pl

[1] Department of General and Coordination Chemistry, Maria Curie-Skłodowska University, Maria Curie-Skłodowska Sq. 2, 20-031 Lublin, Poland

[2] Chair and Department of Medical Chemistry, Medical University, 4A Chodźki Street, 20-093 Lublin, Poland

[3] Laboratory of Bioorganic Synthesis and Analysis, Chair and Department of Medical Chemistry, Medical University, 4A Chodźki Street, 20-093 Lublin, Poland

Introduction

Medicinal substances and drug candidates in both their pure state and in pharmaceutical preparations (tablets, solutions, mixtures, intramuscular or parenteral injections, suppositories, gel, creams, inhalations, depot forms) can be prone to physical changes and undergo chemical, enzymatic and biological ones. It is commonly known that objectionable changes in the solid structure, composition and physicochemical properties of the authorized medicinal products can have remarkable influence on changes in their pharmacological profile (i.e. a decrease in activity or even increased toxicity). Therefore, the manufacturer should guarantee stability of the authorized medicinal product (i.e. the maintenance of its quality, efficacy and safety) during its whole validity period under strictly recommended conditions of storage (including acceptable temperature ranges and humidity limits). Ford and Timmins [1] as well as Giron [2, 3] have reviewed exhaustively the application of thermal analysis and its coupled techniques in the studies of stability and decomposition of a number of pharmaceutical substances.

The paper discusses the thermal behaviour of six anticancer active derivatives of 3-(2-furanyl)-8-aryl-7,8-dihydroimidazo[2,1-*c*][1,2,4]triazin-4(6*H*)-one. Of this set of bioactive substances as the tested compounds there were used 3-(2-furanyl)-8-phenyl-7,8-dihydroimidazo[2,1-*c*][1,2,4]triazin-4(6*H*)-one (**1**), 3-(2-furanyl)-8-(4-methoxyphenyl)-7,8-dihydroimidazo[2,1-*c*][1,2,4]triazin-4(6*H*)-one (**2**), 3-(2-furanyl)-8-(3-chlorophenyl)-7,8-dihydroimidazo[2,1-*c*][1,2,4]triazin-4(6*H*)-one (**3**), 3-(2-furanyl)-8-(4-chlorophenyl)-7,8-dihydroimidazo[2,1-*c*][1,2,4]triazin-4(6*H*)-one (**4**), 3-(2-furanyl)-8-(3,4-dichlorophenyl)-7,8-dihydroimidazo[2,1-*c*][1,2,4]triazin-4(6*H*)-one (**5**), 3-(2-furanyl)-8-(2,6-dichlorophenyl)-

Published online: 27 February 2017

7,8-dihydroimidazo[2,1-*c*][1,2,4]triazin-4(6*H*)-one (**6**) (see Scheme 1).

The majority of investigated compounds (**1**–**3** and **5**, **6**) have been previously identified as capable of revealing both remarkable antiproliferative effects in human tumour cells and lower cytotoxicities for normal human skin fibroblast (HSF) cells [4–6]. Furthermore, previously it was reported that for all these bioactive substances reversed parabolic correlations with remarkable statistical quality were found between their chromatographic partitioning parameters determined on the cholesterol column and pharmacokinetic bioactivity descriptors calculated in silico (that is, their dermal absorption potential, intestinal permeability, binding with human serum albumin, penetration of the blood–brain barrier) [7]. First and foremost, the structure depicted as **6** has shown an important level of selective cytotoxicity for human cervical epithelial carcinoma cells over normal HSF cells in the same effective concentration [6]. Therefore, this bioorganic substance has been disclosed as a promising lead structure for the design of low-toxic anticancer agents [6]. We hope that in the future the above-mentioned small molecule (with the predicted acceptable pharmacokinetic profile) can also be of significant importance with regard to its specific application in a human medicine, that is, the anticipated antitumour field of relevance.

To investigate thermal behaviour of biologically active 3-(2-furanyl)-8-aryl-7,8-dihydroimidazo[2,1-*c*][1,2,4]triazin-4(6*H*)-ones (**1**–**6**), the combined and coupled thermal techniques such as TG–DSC (under air atm.) and TG–FTIR (under N_2 atm.) were used. These techniques allowed us, among others, to determine thermal stability of the compounds and heat of fusion as well as give information about volatile pyrolysis products.

Experimental

Synthesis and short description of compounds 1–6

The synthesis of all the compounds (whose thermal behaviour is presented herein) proceeded according to the [4 + 2] pattern for annulation by condensing the starting 1-arylimidazolidin-2-one hydrazones with 2-oxo-2-furanacetic acid in the boiling *n*-butanol/DMF mixture, as previously patented and published [4–6]. Full structural characterization of the target compounds (IR, ^{1}H NMR and ^{13}C NMR spectral data, elemental analyses), their biological activities, lipophilic behaviour and retention-related hydrophobicity parameters, proved remarkable correlations between the chromatographic partitioning parameters of the newly synthesized compounds and their molecular descriptors and drug-likeness properties determined in silico were previously established and described [4–7].

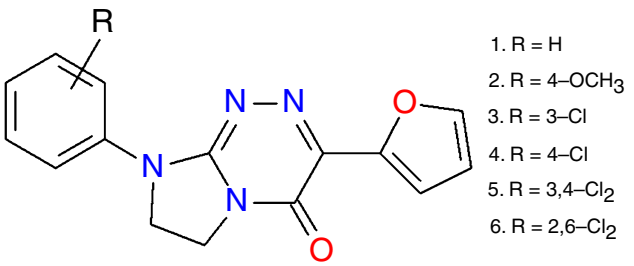

Scheme 1 Structures of the studied compounds

Methods and physical measurements

Thermal stability of studied compounds and their decomposition were determined by Setaram Setsys 16/18 derivatograph under flowing air atmosphere ($v = 0.75$ dm^3 h^{-1}) with a heating rate of 10 °C min^{-1}. The samples (5.34–6.08 mg) were heated in a ceramic crucible at 30–800 °C, and the TG, DTG and DSC curves were recorded. The temperature and heat flow of the instrument were calibrated by the melting point and enthalpy of indium standard. The TG Q5000 analyser (TA Instruments, New Castle, Delaware, USA) interfaced to the Nicolet 6700 FTIR spectrophotometer (Thermo Scientific) was used to perform the TG–infrared spectrometry (TG–FTIR) analysis. The studied compounds (13.60–22.27 mg) were put in open platinum crucible and heated from an ambient temperature (~23–25 °C) to 1000 °C. The analysis was made at a heating rate of 20 °C min^{-1} under nitrogen atmosphere at a flow rate of 25 mL min^{-1}. To minimize condensation of gases along the transfer line, the temperatures were set to 250 and 240 °C in the gas cell and transfer line, respectively. The FTIR spectra were recorded in the spectral range of 600–4000 cm^{-1} with a resolution of 4 cm^{-1} and 6 scans per spectrum.

Results and discussion

The TG–DSC (air) and TG–FTIR (nitrogen) techniques have been used for investigation of thermal behaviour of studied compounds.

Thermal behaviour of studied compounds under air atmosphere

TG and DSC curves, providing information about thermal behaviour of **1**–**6**, are presented in Fig. 1. The melting point onset temperature (T_{onset}), peak temperature (T_{peak}) corresponding to each peak and the enthalpy of fusion

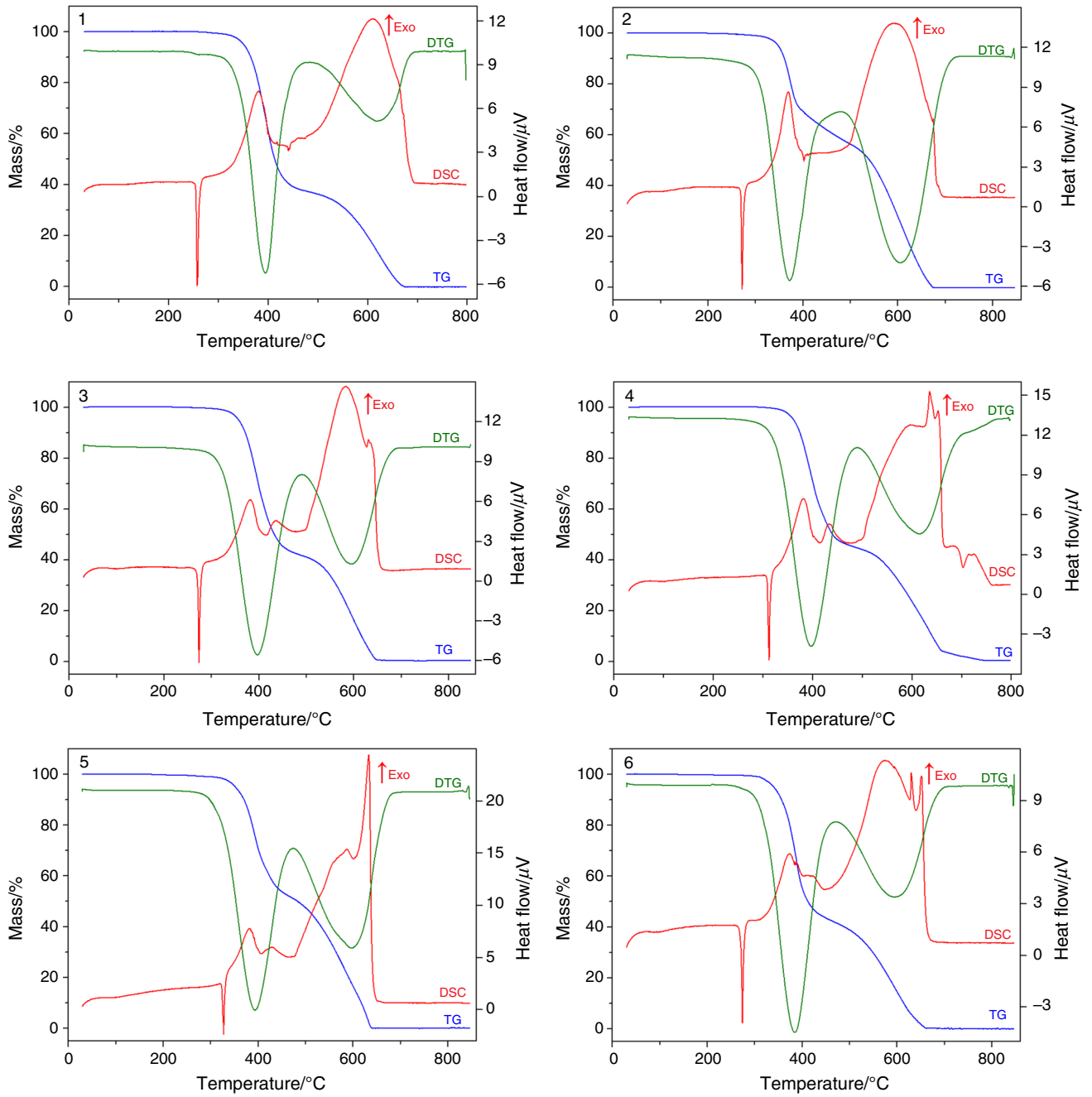

Fig. 1 TG, DTG and DSC curves recorded for **1**–**6** under air atmosphere

taken from the DSC curves for all studied compounds are given in Table 1.

*Thermal behaviour of **1***

Compound **1** is thermally stable under air atmosphere. The first DSC peak appears at 254 °C. This endothermic peak is connected with a lack of mass loss, which is characteristic of the melting process. The melting point observed on the DSC curve (257 °C) is comparable with that determined on a Boetius apparatus (259–261 °C) [6]. This DSC peak is sharp which indicates that compound **1** is a crystalline, pure substance (see Fig. 1). Further heating causes thermal decomposition of the compound proceeding in two steps. The first stage of thermal degradation of **1** starts at 314 °C and is characterized by a fast mass loss rate (63.13%). This step arises from partial degradation and combustion of **1**. The formed intermediate products are unstable and immediately undergo further decomposition process, see Table 2. In the second step of compound decomposition, the

Table 1 Results of the melting process

Compound	T_{onset}/°C	T_{peak}/°C	ΔH_m/J g^{-1}	ΔH_m/kJ mol^{-1}
1	254	257	98.39	27.58
2	269	272	98.75	30.64
3	270	274	101.07	31.81
4	308	312	86.32	27.17
5	323	327	71.97	25.13
6	271	274	87.84	30.67

remaining part of molecule is combusted. The sample fully decomposes at a temperature of approximately 667 °C.

*Thermal behaviour of **2***

Compound **2** exhibits the lowest thermal stability of the studied compounds. A significant change on the TG curve was recorded at 304 °C. The thermal decomposition of **2**, similar to **1**, was preceded by the melting process. On the DSC curve, the endothermic effect is observed as a sharp peak confirming that the analysed compound was synthesised as a pure substance. The melting point read from the DSC curve (272 °C) is close to that previously determined on a Boetius apparatus (275–277 °C) [6]. Thermal decomposition of **2**, similar to that previously described, takes place in two stages, but in contrast to **1** during the first step only 41.50% of the initial mass is lost. The products formed at 478 °C are unstable and undergo further thermal degradation and combustion. This stage corresponds to the complete destruction and combustion of the remaining parts of the compound. Within this step, more than 50% of mass loss is observed (Table 2). The sample fully decomposes at approximately 688 °C.

*Thermal behaviour of **3***

Thermal decomposition of **3** is similar to that observed for **1**. The first effect observed during heating is recorded on the DSC curve at 270 °C as a sharp, endothermic peak, which is not accompanied by a mass loss, and can be attributed to the melting process. As in the case of other compounds, the peak shape indicates that **3** is also a crystalline, pure substance. The melting temperature (274 °C) found from the DSC curve is in good agreement with that determined on a Boetius apparatus (277–279 °C) [6]. Further heating leads to a two-step thermal decomposition of the compound. The first stage of **3** thermal degradation starts with an initial well-separated mass loss of 58.45% between 314 and 493 °C. The second step starts immediately when the first one finished. In this stage, complete combustion and destruction of the remaining part of **3** is observed.

*Thermal behaviour of **4***

Thermal behaviour of **4** is slightly different from those observed for **1–3**. In contrast to the previous compound, the

Table 2 Thermogravimetric data of compounds **1–6**

Compound	Atm	Step 1				Step 2			
		T_{onset}/°C	T_{peak}/°C	T_{final}/°C	Δm/%	T_{onset}/°C	T_{peak}/°C	T_{final}/°C	Δ*m*/%
1	Air	314	394	487	63.08	487	617	667	36.92
	N_2	260	298	567	87.07	–	–	–	–
			412						
2	Air	304	372	478	41.36	478	605	688	58.58
	N_2	311	381	552	58.76	552	801	931	41.10
3	Air	314	393	493	58.45	493	595	655	41.34
	N_2	289	396	491	79.49	–	–	–	–
			414						
4	Air	315	397	486	55.05	486	615	754	44.75
	N_2	286	402	498	80.36	–	–	–	–
5	Air	319	393	469	48.49	469	597	656	51.12
	N_2	290	395	529	74.35	–	–	–	–
6	Air	318	384	460	57.33	460	594	667	42.03
	N_2	264	390	499	81.58	–	–	–	–
			399						

Atm, atmosphere of analysis; T_{onset}, onset degradation temperature; T_{final}, final degradation temperature; T_{peak}, DTG peak temperature (maximum change of mass), Δ*m*, mass loss %

melting process takes place almost simultaneously with the beginning of thermal decomposition of sample. The maximum of endothermic effect associated with the melting process is observed at 312 °C, while the first significant change on the TG curve is recorded at 315 °C. This means that compound **4** was synthesised as a crystalline, pure substance, similar to the above-mentioned compounds. The melting temperature read on the DSC curve is close to that determined on a Boetius apparatus (319–320 °C) [6]. As in the case of compounds **1** and **3**, the first stage of combustion is associated with the loss of more than 50% of the initial mass. The formed products are unstable and immediately undergo further combustion. The sample is fully decomposed at the highest temperature of all studied compounds, i.e. 754 °C.

*Thermal behaviour of **5***

The thermal decomposition of **5** in air, like that of other studied samples, is a two-step process visible on the TG curve (see Fig. 1). As can be seen on the TG curve, thermal degradation of compound **5** starts at 319 °C and less than 50% of the initial mass is lost. At the beginning of thermal decomposition on the DSC curve at 323 °C, an endothermic effect is observed. This peak is associated with the melting process. The enthalpy of fusion calculated from the DSC peak is 25.13 kJ mol^{-1}. This value is the lowest of all the studied compounds (see Table 1) which can be a result of two overlapping effects, i.e. the endothermic effect of melting process and the exothermic effect of sample combustion. This does not enable clearly determination of the heat of fusion. We attempted to obtain better separation of these two peaks conducting the analysis with a lower heating rate (2.5 K min^{-1}), but the profile of the DSC curve was the same making it impossible to designate clearly the fusion heat. The melting temperature (327 °C) found from the DSC curve is slightly different from that determined on a Boetius apparatus (343–344 °C) [6], but the shape of peak indicates that compound **5** was synthesised as a pure one. The differences between these values can be the result of measurement conditions. The second stage, which starts immediately after the first one, is connected with further destruction and combustion of the remaining parts of the compound. The sample is fully decomposed at 656 °C.

*Thermal behaviour of **6***

Thermal behaviour of **6** is similar to that of **1** and **3**. The first change during the heating of the sample was recorded on the DSC (at 271 °C) curve as a sharp, endothermic peak. The TG curve does not show any change of the mass which confirms that it is the peak of the melting process. The melting temperature read from the DSC curve (274 °C) is close to that previously determined on a Boetius apparatus (279–281 °C) [6]. Next, the compound undergoes a two-stage decomposition process. The first step is observed at 318–460 °C, and almost 60% of compound is combusted. The formed products are unstable and undergo further decomposition and combustion. The sample fully decomposes at a temperature of approximately 667 °C.

*Comparison of the thermal behaviour of **1–6** in air*

The TG–DSC curves show that compounds **1–6** are thermally stable under air stream up to ~250 °C. For almost all studied compounds (except **5**), the first changes are recorded on the DSC curves and associated with melting processes. In the case of **5**, melting processes are preceded by decomposition. As a general rule, melting points do generally increase with the increasing molecular mass and symmetrical molecules in the crystalline form have higher melting points compared with those of similar structure but with a lower symmetry [8–11]. The structures of the studied compounds are composed of 3-(2-furanyl)-8-aryl-7,8-dihydroimidazo[2,1-*c*][1,2,4]triazin-4(6*H*)-one unit and differently substituted benzene fragments. Therefore, it can be assumed that the substitution at the benzene moiety will affect the melting process of the studied compounds. The melting points for the studied compounds change in the following order: $\mathbf{1} < \mathbf{2} \approx \mathbf{3} \approx \mathbf{6} < \mathbf{4} < \mathbf{5}$. Compound **1** has the smallest molar mass, and therefore it should have the lowest melting point which is in agreement with the obtained results. Compounds **3** and **4** belong to the monochloro-substituted phenyl derivatives where the more symmetrical *para* analogue (**4**) has a higher melting point than the *meta*-chloro compound. With regard to the dichloro-substituted phenyl derivatives, more symmetrical compound **6** has a lower melting point than that of **5**. This derogation from the general rule can be associated with the structure of these compounds. In the case of compound **5,** it is more likely that the electronegative Cl atoms can be engaged in polar interactions like π–π or H-bonding which can increase the melting point [8–10].

Decompositions of **1–6** are a two-step process under air atmosphere. The first mass loss for the compounds (except **2**) is observed at approximately similar temperatures, i.e. above 310 °C, but the combustion of the studied compounds takes place in different ways as evidenced by their mass losses. Only thermal decomposition of **2** starts below the above-mentioned temperature. The first stage is associated with partial combustion of the studied samples, and almost for all compounds (except **2** and **5**) more than 50% of the initial mass undergoes degradation.

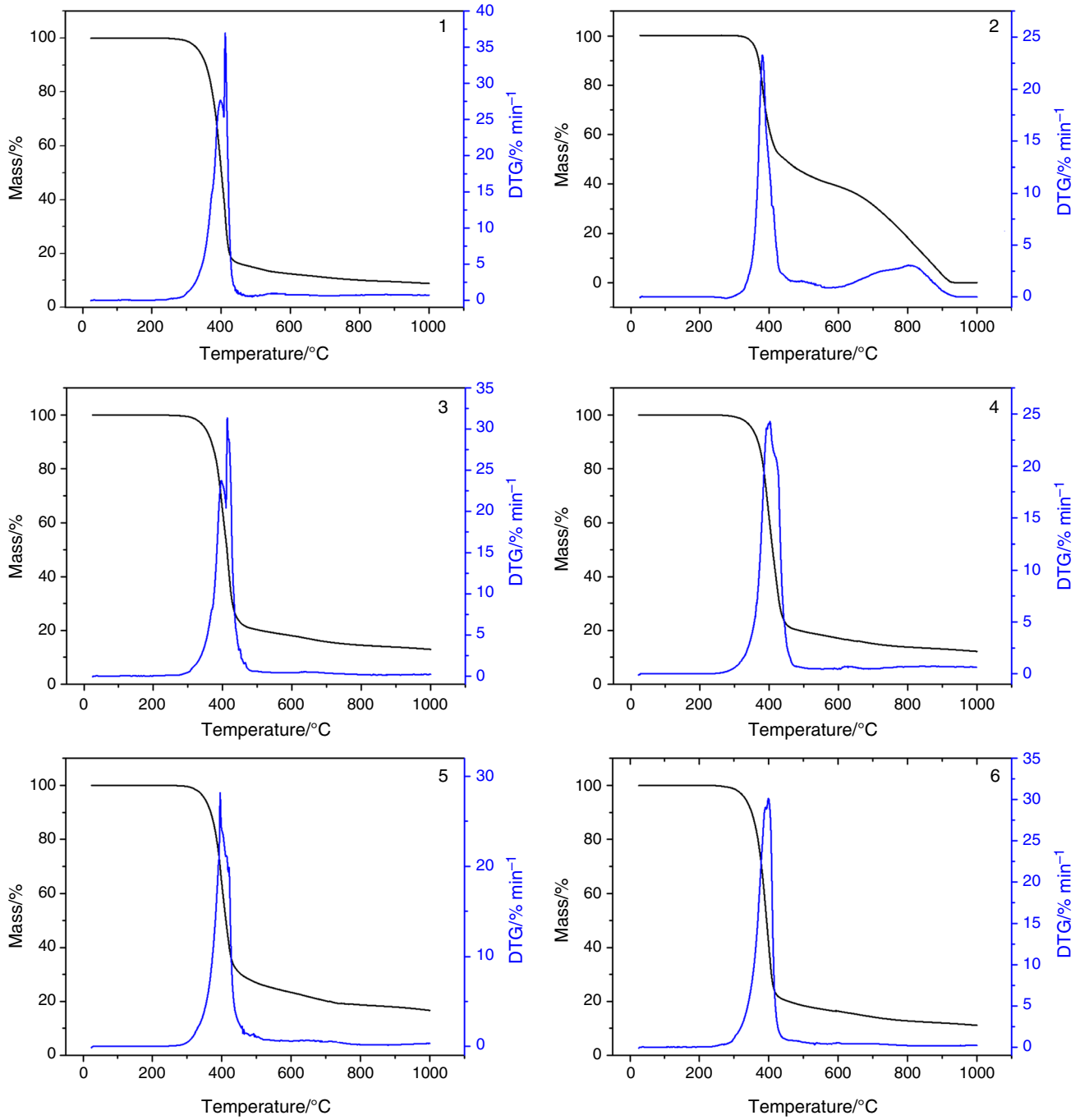

Fig. 2 TG and DTG curves of **1–6** recorded in nitrogen atmosphere

Thermal behaviour of 1–6 under nitrogen atmosphere

Thermal behaviours of compounds have been also studied in nitrogen atmosphere, and they differ from those recorded in air. As can be seen from Fig. 2, the pyrolysis processes proceed in one major mass loss step under measurement conditions for almost all compounds (except **2**), and in contrast to the thermal decomposition in air atmosphere, these processes are not finished. Compounds **1**, **3–6** are thermally stable up to 260–311 °C and then decompose with the initial mass loss in the range 74.35–80.36% (see Table 2). The further heating causes slow decomposition and pyrolysis of some remaining parts of the compounds, but it is not clearly marked on the DTG curves of **1**, **3–6**. The differences in mass losses after first decomposition

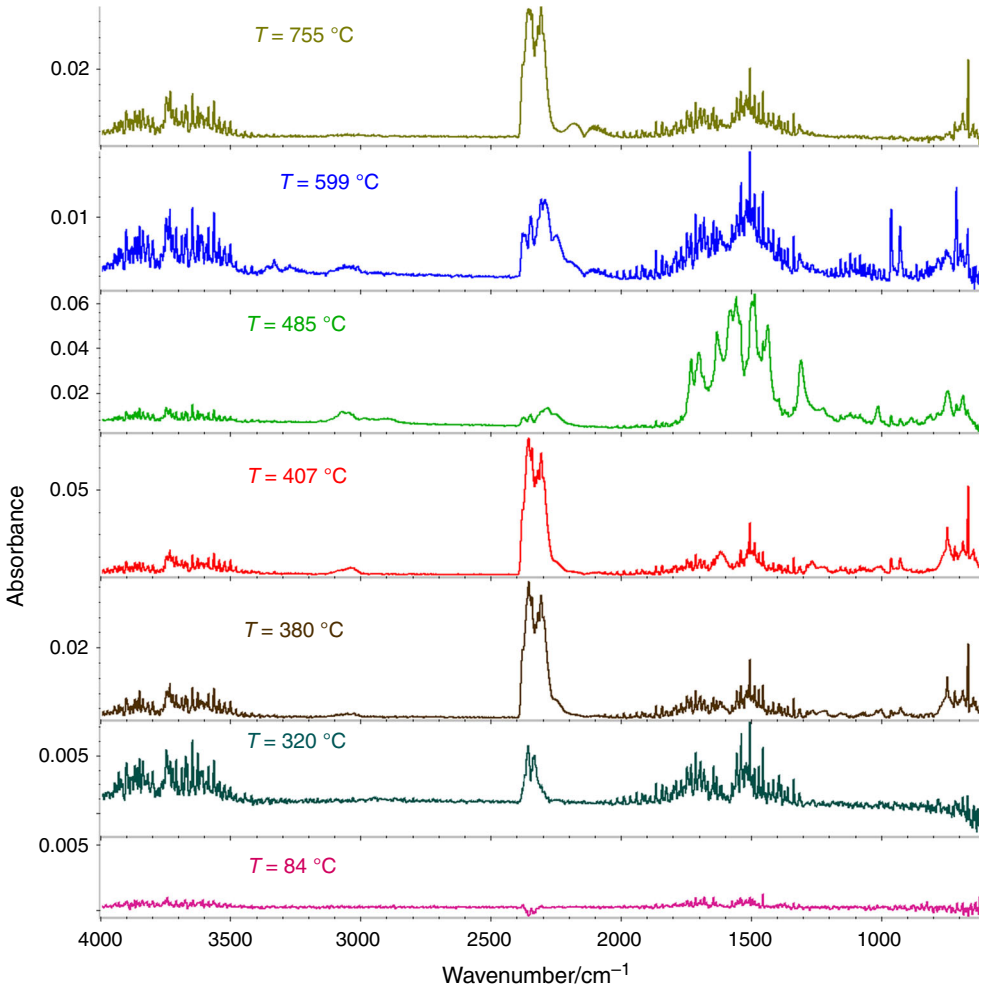

Fig. 3 Some FTIR spectra of volatile products of thermal decomposition of **1** recorded at different temperatures

step of **1**, **3**–**6**, which are marked with a peak on the DTG curves, and the final temperature (1000 °C) are 4.1–9.0%. The decomposition of **2** in nitrogen is a two-step process as visible on the TG curves (Fig. 2). The first stage of thermal degradation of **2** starts at 311 °C. In contrast to the thermal decomposition of **2** in air, this step is characterized by the fast mass loss rate (58.76%) and is associated with partial degradation and pyrolysis. The formed intermediate products are unstable and immediately undergo further decomposition processes. In the second step of compound decomposition, the remaining part is burnt. The sample fully decomposes at a temperature of approximately 931 °C. Together with the TG analysis under nitrogen atmosphere, the FTIR spectra of gaseous products were recorded. The FTIR spectra of gaseous products evolved during the pyrolysis of compounds **1**, **2** and **5** are presented in Figs. 3–5. At the beginning of the decomposition process of all studied compounds, the main gaseous products emitted at around 320–360 °C are identified as: H_2O (4000–3450 and 1950–1300 cm^{-1}) [10–14] and CO_2 (peaks at 2450–2300 and 750–600 cm^{-1}) [10–14]. Then the pyrolysis of compounds proceeds in three different ways (Scheme 2).

On the FTIR spectra of the evolved gas phase of compounds **1**, **3** and **4** around 380–390 °C, there appear bands characteristic of: (a) NH_3 (several bands with two characteristic maxima at 966 and 931 cm^{-1}) [10, 11, 14, 15]; (b) HNCO and its methyl and ethyl derivatives (RNCO, 3508 and 2300–2180 cm^{-1}) [10–13, 15]; (c) aniline or its derivatives such as: aniline (3413 cm^{-1} (ν(NH)); 3089 and 3041 cm^{-1} (ν(CH)); 1622 cm^{-1} (δ(NH)); 1506 cm^{-1} ($\nu(C_{ar}{=}C_{ar})$; 1271 cm^{-1} (ν(CN)) and 749 cm^{-1} (ω(NH) for **1**), *m*-chloroaniline (3416 cm^{-1} (ν(NH)), 3064 cm^{-1} ($\nu(C_{ar}H)$); 1625 cm^{-1} (δ(NH)); 1581 and 1486 cm^{-1} ($\nu(C_{ar}{=}C_{ar})$; 1310 and 1236 cm^{-1} (ν(CN)); 1085 cm^{-1} ($\beta(C_{ar}H)$); 887 and 766 cm^{-1} ($\gamma(C_{ar}H)$); 669 cm^{-1} (ν(CCl) for **3**) and *p*-chloroaniline (3594 and 3404 cm^{-1} (ν(NH)), 3040 cm^{-1} ($\nu(C_{ar}H)$); 1636 cm^{-1} (δ(NH)); 1489 cm^{-1} ($\nu(C_{ar}{=}C_{ar})$; 1456 cm^{-1} ($\nu(C_{ar}{=}C_{ar})$; 1274 cm^{-1} (ν(CN)); 1007 cm^{-1} (ring); 816 cm^{-1} ($\gamma(C_{ar}H)$); 669 cm^{-1} (ν(CCl) for **4**) [10, 11]. Further heating increases the intensity of the bands characteristic of aniline or its derivatives as well as

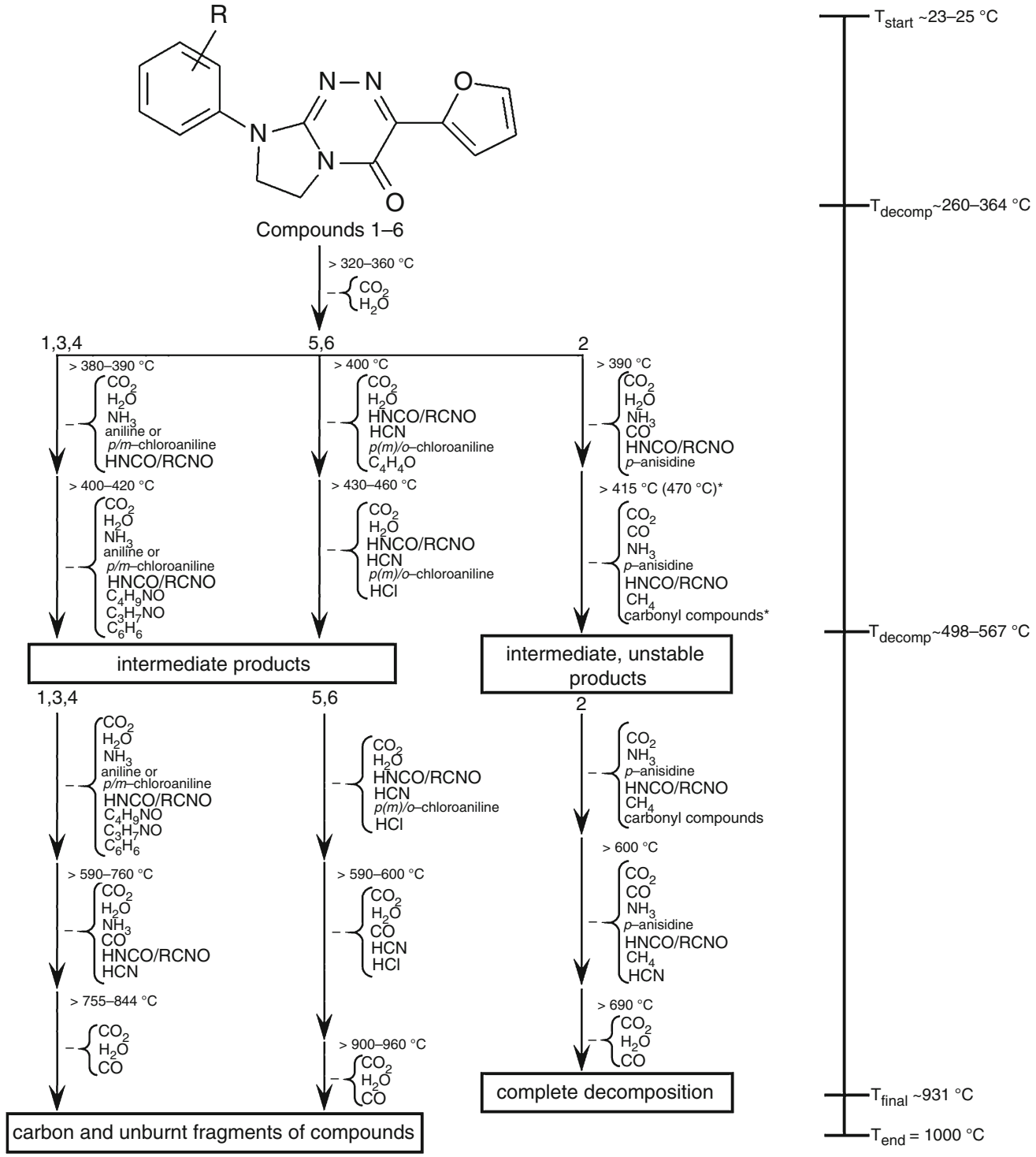

Scheme 2 Gaseous species evolved during the thermal decomposition processes in nitrogen atmosphere with the temperature ranges

there appear new bands associated with pyrolysis of the benzene unit and fused ring, such as: benzene (C_6H_6), *N*,*N*-dimethylacetamide (C_4H_9NO) or *N*,*N*-dimethylformamide (C_3H_7NO). The bands assigned to benzene occur in the ranges 3150–3000, 1550–1450 and 1050–1000, and at 692, 672 and 653 cm^{-1} [14, 17]. The most characteristic, qualitative bands for C_4H_9NO are observed at 2982 cm^{-1} ($\nu(CH_3)$); 1697 cm^{-1} ($\nu(C{=}O)$); 1455 and 1404 cm^{-1} ($\delta(CH_3)$); 1271 cm^{-1} ($\nu(CN)$); 998 cm^{-1} ($\gamma(CH_3)$) [18, 19], while those associated with *N*,*N*-dimethylformamide are recorded at 2982 cm^{-1} ($\nu(CH_3)$); 2898 cm^{-1} ($\nu(CH)$); 1733 cm^{-1} ($\nu(C{=}O)$); 1373 cm^{-1} ($\delta(CH_3)$); 1269

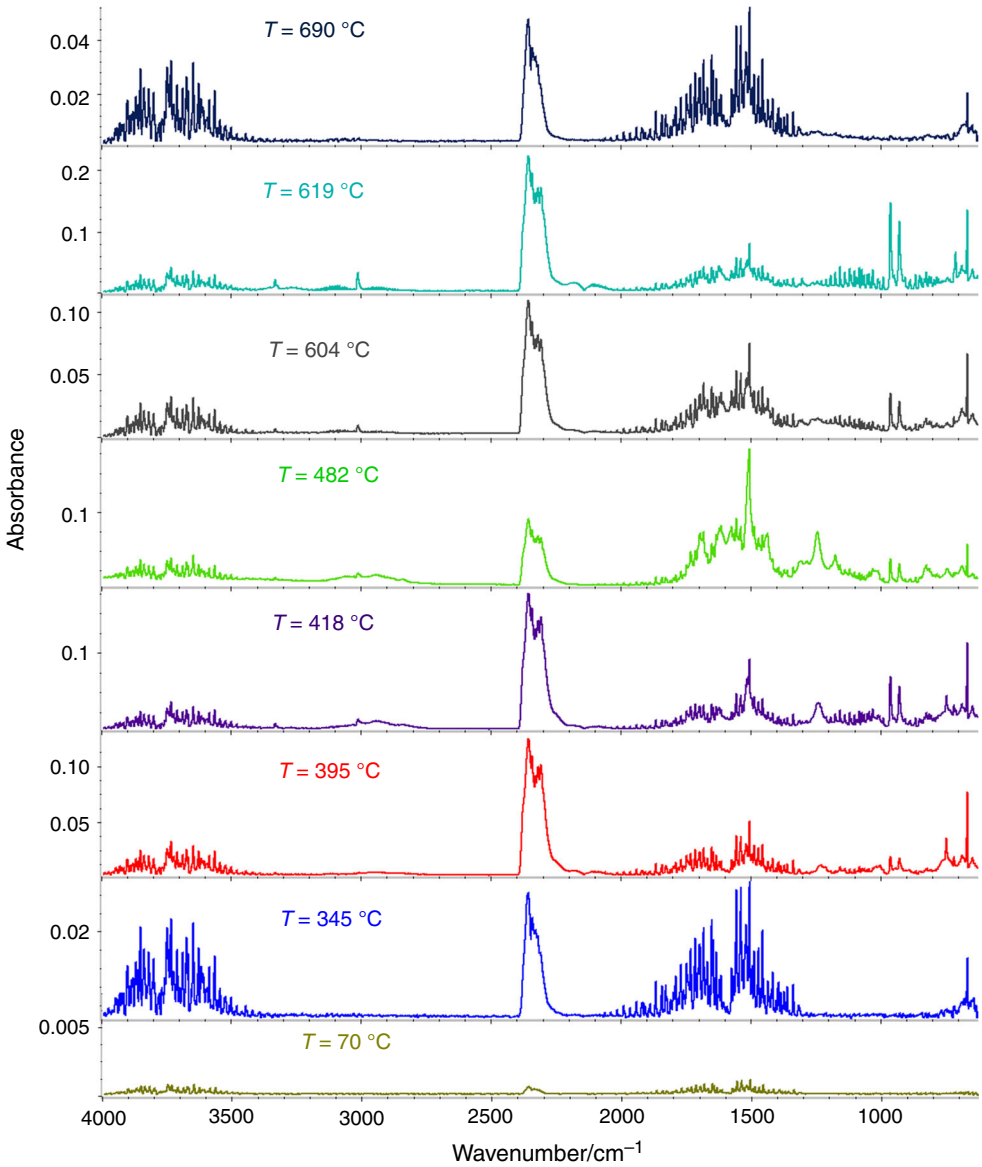

Fig. 4 Chosen FTIR spectra of volatile products of thermal decomposition of **2** recorded at different temperatures

and 1246 cm^{-1} (ν(CN)); 1085 cm^{-1} ($\rho(CH_3)$) [18–20]. At ~599 °C (1), ~765 °C (3) and ~740 °C there were identified the following molecules in a mixture of gaseous products: H_2O, CO_2, NH_3, CO, hydrogen cyanide (HCN) and HNCO and its derivatives. The double peaks corresponding to CO are recorded in the range at 2050–2275 cm^{-1}, whereas the vibrations assigned to HCN occur at 3336, 3273, 714 cm^{-1} [10, 11]. The evolved gaseous products, which were observed above 755–844 °C, are CO_2, CO and H_2O.

In the case of compound **2**, similar to the previously described ones, the further pyrolysis process (above 390 °C) is associated with emission of CO_2, H_2O, NH_3, HNCO and *p*-anisidine as well as CO. The most characteristic, qualitative bands for *p*-anisidine are recorded at 2948 and 2844 cm^{-1} (ν(CH)); 1622 cm^{-1} (δ(NH)); 1508 cm^{-1} ($\nu(C_{ar}{=}C_{ar})$; and 1247 cm^{-1} (ν(CN)) [10, 11]. Further heating causes an increase in the emission of these gaseous species, especially anisidine and the new products, methane (in the range 3175–2900 cm^{-1} with a characteristic maximum at 3016 cm^{-1} [10, 11, 13, 16]) and the carbonyl compounds (bands at ~1699 and ~1684 cm^{-1} [10, 11, 21]), are observed. At higher temperature, the HCN bands are also recorded in the FTIR spectra at 604 °C. Above 690 °C in the FTIR spectra of evolved volatile pyrolysis products, only bands of CO_2 and H_2O were recorded, see Fig. 4.

In contrast to the previously discussed compounds, in FTIR spectra of **5** and **6** the bands characteristic of NH_3 are not observed. Heating above 400 °C, besides CO_2 and H_2O, causes formation of the following gases: HCN, HNCO and its derivatives, chloroaniline (*meta* and *para* for

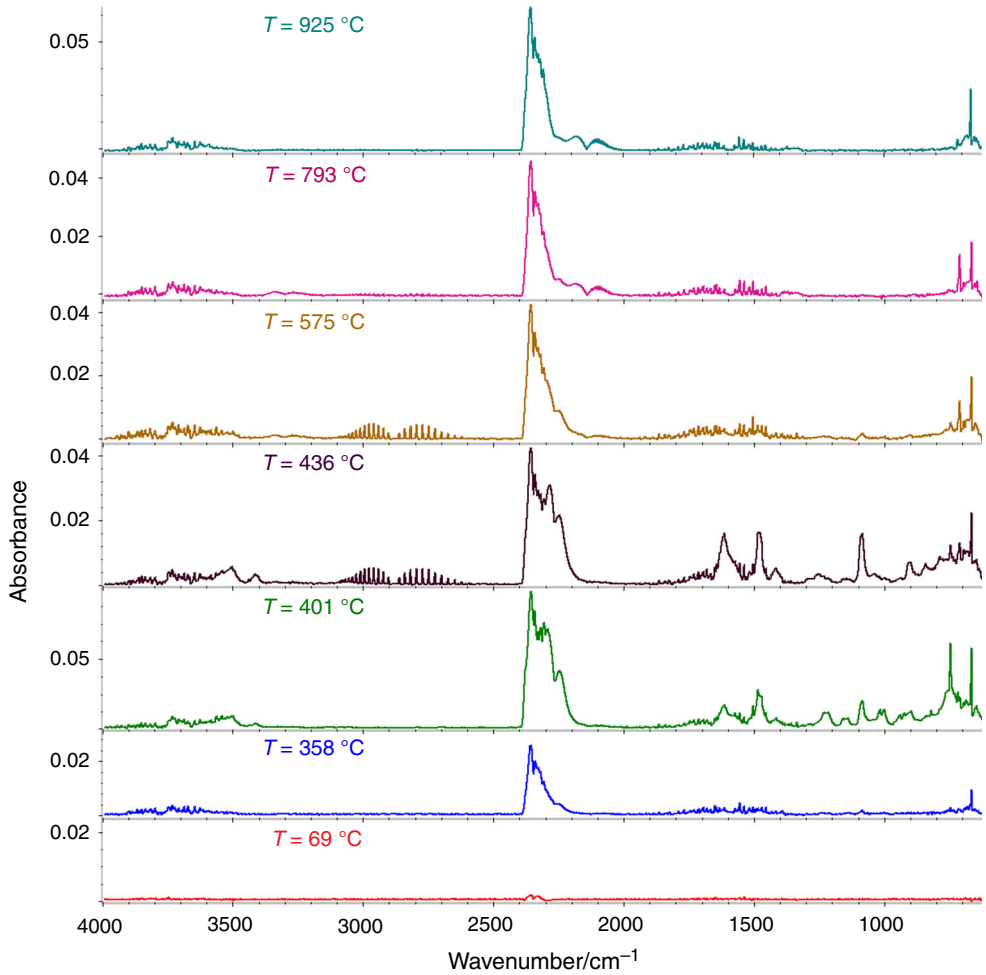

Fig. 5 FTIR spectra of volatile products of thermal decomposition of **6** recorded at different temperatures

5 and *ortho* for **6**) and furan and its derivatives. The most characteristic, qualitative bands for furan are recorded at 1577, 1503 and 1489 cm^{-1} (ν(C=C)); 1161 cm^{-1} (ν(CO)); 1147 cm^{-1} (ρ(CH)); 1088 cm^{-1} (ν(CO) + ν(C=C)); 1020 and 1005 cm^{-1} (ρ(CH) + ν(CO)); 758, 749 and 733 cm^{-1} (ω(CH)) [22]. With the increasing temperature the new gas product, hydrogen chloride (several bands in the range 3100–2640 cm^{-1} [23, 24]), is emitted, whereas furan disappears. The HNCO derivatives, and chloroaniline bands are not found in the FTIR spectra of evolved volatile pyrolysis products at 600 °C (**5**) and 590 °C (**6**). At the end of pyrolysis, [960 °C (**5**) and 900 °C (**6**)] only CO, CO_2 and H_2O are observed in the mixtures of emitted gases (see Fig. 5).

Conclusions

In this paper, the thermal behaviour of six anticancer active derivatives of 3-(2-furanyl)-8-aryl-7,8-dihydroimidazo[2,1-*c*][1,2,4]triazin-4(6*H*)-one has been discussed. The presented compounds exhibit high thermal stability which is an important factor for prospective medical application as well as during the storage and processing by pharmaceutical industry. The sharp DSC peaks associated with the melting process indicate that they are crystalline, pure substances. Such compounds exhibit a higher chemical and physical stability than the amorphous substances. The TG–FTIR analysis supports the DSC studies, i.e. the compounds have been synthesised as pure and not hygroscopic, as well as there are no residual solvents in their structure. The TG–FTIR analysis also confirmed formation of various compounds during pyrolysis. The main volatile decomposition products of pyrolysis are the following gases: CO_2, CO, NH_3, HCN, HNCO (and its derivatives), aniline or its derivatives, methane (for **2**) and HCl (for **5** and **6**).

References

1. Ford JL, Timmins P. Pharmaceutical thermal analysis: techniques and applications. Chichester: Ellis Horwood; 1989.
2. Giron D. Thermal analysis of drugs and drug products. In: Swarbrick J, Boylan JC, editors. Encyclopedia of pharmaceutical technology, vol. 15. New York: Marcel Dekker; 1995. p. 1.
3. Giron D. Applications of thermal analysis and coupled techniques in pharmaceutical industry. J Therm Anal Calorim. 2002;68: 335–57.
4. Sztanke K, Sztanke M, Pasternak K. Derivatives of 3-(2-furanyl)-7,8-dihydroimidazo[2,1-*c*][1,2,4]triazin-4(6*H*)-one substituted with phenyl, alkylphenyl, alkoxyphenyl and process for the preparation thereof. PL Patent 212447, 2012; Appl. No. 201003 93191, 2010.
5. Sztanke K, Sztanke M, Pasternak K. 3-(2-Furanyl)-7,8-dihydroimidazo[2,1-*c*][1,2,4]triazin-4(6*H*)-ones substituted with mono- or dichlorophenyl and process for the preparation thereof. PL Patent. 212442, 2012; Appl. No. 20100393192, 2010.
6. Sztanke K, Tuzimski T, Sztanke M, Rzymowska J, Pasternak K. Synthesis, structure elucidation, determination of the lipophilicity and identification of antitumour activities in vitro of novel 3-(2-furanyl)-8-aryl-7,8-dihydroimidazo[2,1-*c*][1,2,4]triazin-4(6*H*)-ones with a low cytotoxicity towards normal human skin fibroblast cells. Bioorg Med Chem. 2011;19:5103–16.
7. Janicka M, Sztanke M, Sztanke K. Reversed-phase liquid chromatography with octadecylsilyl, immobilized artificial membrane and cholesterol columns in correlation studies with in silico biological descriptors of newly synthesized antiproliferative and analgesic active compounds. J Chromatogr A. 2013;1318:92–101.
8. Brown RJC, Brown RFC. Melting point and molecular symmetry. J Chem Educ. 2000;77:724–31.
9. Rao SP, Sunkada S. Making sense of boiling points and melting points. Resonance. 2007;12:43–57.
10. Bartyzel A, Sztanke M, Sztanke K. Thermal studies of analgesic active 8-aryl-2,6,7,8-tetrahydroimidazo[2,1-*c*][1,2,4]triazine-3,4-diones. J Therm Anal Calorim. 2016;123:2053–60.
11. Bartyzel A, Sztanke M, Sztanke K. An insight into the thermal behaviour of biologically active 8-aryl-4-oxo-4,6,7,8-tetrahydroimidazo[2,1-*c*][1,2,4]triazine-3-carbohydrazides. J Anal Appl Pyrolysis. 2016;121:138–45.
12. Plis A, Kotyczka-Morańska M, Kopczyński M, Łabojko G. Furniture wood waste as a potential renewable energy source. A thermogravimetric and kinetic analysis. J Therm Anal Calorim. 2016;125:1357–71.
13. Bartyzel A. Synthesis, crystal structure and characterization of manganese(III) complex containing a tetradentate Schiff base. J Coord Chem. 2013;66:4292–303.
14. Łyszczek R, Ostasz A, Bartyzel A, Lipke A. Thermal, spectroscopic and luminescence investigations of lanthanide(III) coordination polymers based on V-shaped 4,4′-sulfonyldibenzoic acid. J Anal Appl Pyrolysis. 2015;115:370–8.
15. Girods P, Dufour A, Rogaurne Y, Rogaurne C, Zoulalian A. Pyrolysis of wood waste containing urea-formaldehyde and melamine-formaldehyde resins. J Anal Appl Pyrolysis. 2008; 81:113–20.
16. Bartyzel A, Kaczor A. The formation of a neutral manganese(III) complex containing a tetradentate Schiff base and a ketone—synthesis and characterization. J Coord Chem. 2015;68:3701–17.
17. Bartyzel A. Synthesis, thermal study and some properties of N_2O_4-donor Schiff base and its Mn(III), Co(II), Ni(II), Cu(II) and Zn(II) complexes. J Therm Anal Calorim. 2016;. doi:10.1007/s10973-016-5804-0.
18. Chalapathi VV, Ramiah KV. Normal vibrations of *N*,*N*-dimethylformamide and *N*,*N*-dimethylacetamide. Proc Indian Acad Sci Sect A. 1968;68:109–22.
19. Duce C, Spepi A, Pampaloni G, Piccinelli F, Tiné MR. Thermal decomposition of metal *N*,*N*-dialkylcarbamates. A TG–FTIR study. J Therm Anal Calorim. 2016;123:1563–9.
20. Ståkhandske CMV, Mink J, Sandström M, Pápai I, Johansson P. Vibrational spectroscopic and force field studies of *N*,*N*-dimethylthioformamide, *N*,*N*-dimethylformamide, their deuterated analogues and bis(*N*,*N*-dimethylthioformamide)mercury(II) perchlorate. Vib Spectrosc. 1997;14:207–27.
21. Wang S, Hu Y, Wang Q, Xu S, Lin X, Ji H, Zhang Z. TG–FTIR–MS analysis of the pyrolysis of blended seaweed and rice husk. J Therm Anal Calorim. 2016;126:1689–702.
22. El-Azhary AA, Hilal RH. Vibrational analysis of the spectra of furan and thiophene. Spectrochim Acta A. 1997;53:1365–73.
23. Ledeţi I, Fuliaş A, Vlase G, Vlase T, Bercean V, Doca N. Thermal behaviour and kinetic study of some triazoles as potential anti-inflammatory agents. J Therm Anal Calorim. 2013;114:1295–305.
24. Ambrozini B, Cervini P, Cavalheiro ÉTG. Thermal behavior of the β-blocker propranolol. J Therm Anal Calorim. 2016;123: 1013–7.